Quantification of local blood flow characteristics in microfluidic applications

E. Kaliviotis[1], J.M. Sherwood[2], J. Dusting, S. Balabani[3]

[1]*Department of Mechanical Engineering and Material Science and Engineering, Cyprus University of Technology, Cyprus*
[2]*Department of Bioengineering, Imperial College London, UK*
[3]*Department of Mechanical Engineering, University College London, UK*

Abstract

Advances in microfluidic applications have made it possible to design microsystems in which various processes, including diagnostics and fundamental research in biofluids, can be performed. In the majority of the studies the effect of red blood cell aggregation in blood flow characteristics has not received much attention and the relationship between the local microstructure and local flow characteristics has not been investigated extensively. In this work local velocity, local aggregation and local hematocrit of human red blood cells (RBC) have been simultaneously, resolved and quantified in a microchannel. The experimental system involved simple brightfield microscopy, a pressure driven microfluidic system, and RBCs suspended in Dextran and phosphate buffer saline solutions to control the aggregation intensity. Local aggregation characteristics were investigated at bulk and local levels using statistical and edge-detection image processing techniques. Aggregation intensity was found to strongly correlate with local variations in velocity in both the central and wall regions. The results suggest a combined effect of haematocrit and velocity distributions on local aggregation characteristics and showed that using multiple methods for aggregation quantification, could help towards a robust characterisation of the structural properties of the fluid

Keywords: Blood flow, red blood cell aggregation, micro-PIV, image processing techniques

1. Introduction

Erythrocyte aggregation occurs mainly in the presence of the protein fibrinogen and when shear stresses are sufficiently low, and is intense in various pathological conditions [1,2,3,4]. The intrinsic properties of the erythrocytes also influence erythrocyte aggregation independently of the suspension biochemistry [5,6]. Aggregated cells form a cellular tube-like arrangement (so called rouleaux), which is very flexible due to the cells' deformability. Larger aggregates, and at low shear rates a three dimensional cellular network, result from combinations of rouleaux [7]. The formation of aggregates affect the flow of blood and the viscosity of the fluid [8,9,10,11]. Elevated viscosity can result in the hyperviscosity syndrome and other complications [12,13,14,15,16,17].

Erythrocyte aggregation and the microstuctural changes it causes at various RBC concentrations and flow conditions have been examined and quantified by indirect techniques, such as erythrocyte sedimentation rate (ESR), light reflection/transmission, ultrasonic, or electrorheology techniques are popular due to their practicality and low cost [18,19]. Optical microscopy and image analysis techniques offer a direct approach for an the characterisation erythrocyte aggregation. The characteristics which are examined by utilising image analysis techniques include the area covered by the cells compared to the total image area [1], the size of the plasma gaps [20] a network index, which was found to increase linearly with the aggregation extent [21], etc. The assessment of aggregation characteristics takes place at either static or steady flow conditions, and usually for steady flow studies the level of hematocrit is kept very low for image quality purposes.

The main technique for measuring blood flow velocity is the Particle Image Velocimetry (PIV) technique [22,23]; it is an image based method in which pairs of images are divided into smaller interrogation windows and correlated. Correlated interrogation windows result in the calculation of the

average velocity of the particles present. Micro-PIV and micro-PIV-based techniques are variations of the classic PIV and aim to microscale flows [22], suitable for the characterisation of blood flows [24,25,26,27,28,29,30,31). The present

study reports results on local measurements of erythrocyte aggregation, haematocrit and velocity for blood flow in a rectangular microchannel under different flow conditions, in order to enhance understanding on the flow of blood.

2. Methods

The details of the methodology can be found in Kaliviotis etal [21] and only a brief description will follow below.

2.1 Sample preparation

Samples were acquired with the approval of the Southeast London Ethics Committee (ref: 10/H0804/21)). Blood was collected from healthy volunteers into vacuum tubes (BD, 367873) preloaded with 1.8 mg/ml EDTA. The erythrocytes were washed twice in Phosphate Buffered Saline (PBS), centrifuged at 3000 rpm, and suspended in PBS containing Dextran 2000 (5g/L). The hematocrit was adjusted 25% by volume as appropriate for the microchannel diameter [32,33,34]. For consistency all experiments were conducted with a single sample.
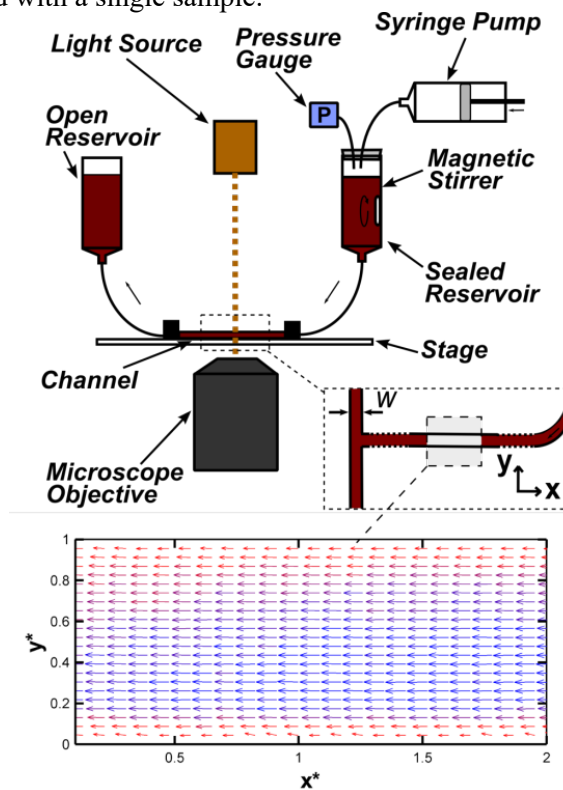

Fig. 1. A schematic represantation of the flow system

2.2 The flow system

Polydimethylsiloxane (PDMS) microchannels, fabricated using photolithography (Epigem, Redcar, UK), were mounted on a stage above an inverted microscope and perfused via a simple microfluidic system, as shown in Figure 1. The sample was perfused through the microchannel by generating a pressure drop between the sealed inlet reservoir and the open outlet reservoirs. The air pressure in the inlet reservoir was controlled with a syringe pump and pressure gauge. In order to minimise effects of erythrocyte sedimentation, which is particularly pronounced for aggregating samples, the fluid in the inlet reservoir was continuously mixed with a magnetic stir bar and all tube lengths were kept to a minimum.

For the cases studied, the reservoir pressure was set to a value between $0 \leq P_0 \leq 3.9$ kPaG, which provided a range of non-aggregating and aggregating conditions within the velocity range occurring in the

human microcirculation [35]. Experimental P_0 values were set by displacing the syringe plunger by an appropriate amount over a period of 10 s. Between cases the pressure was returned to $P_0 = 20$ kPaG to

disaggregate the cells and ensure a uniform initial haematocrit profile. All experiments were conducted at room temperature.

The width and depth of the channel in all regions were $w = 200\mu$m and $d = 50\mu$m, respectively. For the current experiments, a straight region of the channel approximately $90w$ downstream of the end of the curved section and approximately $60w$ upstream of the bifurcation, was chosen for the interrogation region. The tube haematocrit was estimated to be 19.5% using the conversion ratio defined by Barbee and Cokelet [36] and based on the hydraulic diameter (80 μm). The flow rates where estimated based on the velocity measurements and found to be within the 2.84 to 69.6 µl/h for the dextran cases. The corresponding pseudo shear rates, calculated as $\dot{\gamma} = \bar{U}/d$ ($\bar{U}$ is the mean velocity), found to be in the range 0.5 to 31 s^{-1} for the dextran cases.

2.3 Microscopy and microPIV system

The primary Micro-PIV experiments were performed using brightfield illumination with a 10x objective. Images of 1280×384 pixels were recorded using a IDT X3 CMOS camera (Tallahassee, USA) at a spatial resolution of 0.52 μm/pixel. A halogen light-source was used to illuminate the imaged region of the channel from above. For each data set, 100 images of 100μs exposure were acquired over a period of approximately 43 ms at a frame rate of 2300 Hz. Data sets were obtained every second for exactly 60 s after adjusting $P0$. The image acquisition rate was selected to allow measurement of the highest flow rates, meaning that the gap between PIV image pairs (Dt) required adjustment by skipping frames between images so that the pixel displacement between frames was approximately 5-8 pixels for all cases. Images were processed with two different interrogation window sizes (32×32 pixels and 16×16 pixels), with an overlap of 50% in each case

3. Results

3.1 Mean flow characteristics

As the flow rate was not measured directly, each case is described by its Reynolds number, defined by $Re = \bar{U}D/n$, where $\bar{U}$ is the average velocity measured from the PIV data, D is the hydraulic diameter of the channel (80μm) and n is the kinematic viscosity of the liquid phase. The Reynolds number ranged between $0 \leq Re \leq 0.52$ over the cases studied, which is typical of viscous dominated flows found in the microvasculature [35]. Due to its superior temporal resolution and its usefulness for obtaining instantaneous information regarding aggregation characteristics, brightfield microscopy(BM) PIV was the primary flow measurement technique used for the current investigation, however fluorescent microscopy (FM) PIV was used for additional confirmation of the mean velocity field in the liquid phase. Figure 1 includes a velocity field measured using FMPIV, corresponding to a non-aggregating case. The x and y co-ordinates of the velocity field are normalised by w, which is notated using asterisks. For clarity, every second vector in the x direction has been omitted. The velocities are close to uniform across the channel, although the peak velocity consistently occurs around $y \approx 0.4$. This slight asymmetry in the flow profiles is caused by the upstream curved section of channel.

3.2 Effect of aggregation on flow profiles in microchannel

Images of erythrocytes acquired for three selected flow cases are shown in Figure 2. All image sets were captured at approximately 60 s after adjusting P_0. Fig.2(a) corresponds to $Re = 0.52$, the maximum of the measurement range, and represents a state in which the erythrocytes are completely disaggregated. Individual cells are clearly visible, and there is a slight gradient in the concentration of cells due to axial migration of cells away from the walls, however the image appears relatively uniform in intensity. For $Re = 0.02$, shown in Fig. 2(b), red blood cell aggregation is apparent. This trend is expected as the shear magnitudes scale closely with Re, and aggregation is associated with lower shear rates. While the shear rate varies throughout the channel, overall levels decrease with mean velocity $\bar{U}$. The relationship between aggregation and flow rate was highlighted by calculating four simple parameters relating to the brightness and contrast of the image. These include the mean pixel (intensity) value ($\bar{I}$), the mean pixel value of the brightest 10% of pixels ($\bar{I}'$), the standard deviation of the pixel value (σ_I), and the number of saturated pixels (n_s). Gaps between erythrocytes caused by aggregation lead to a greater transmission of light through the channel, which results in an increase in brightness, while contrast is further increased by

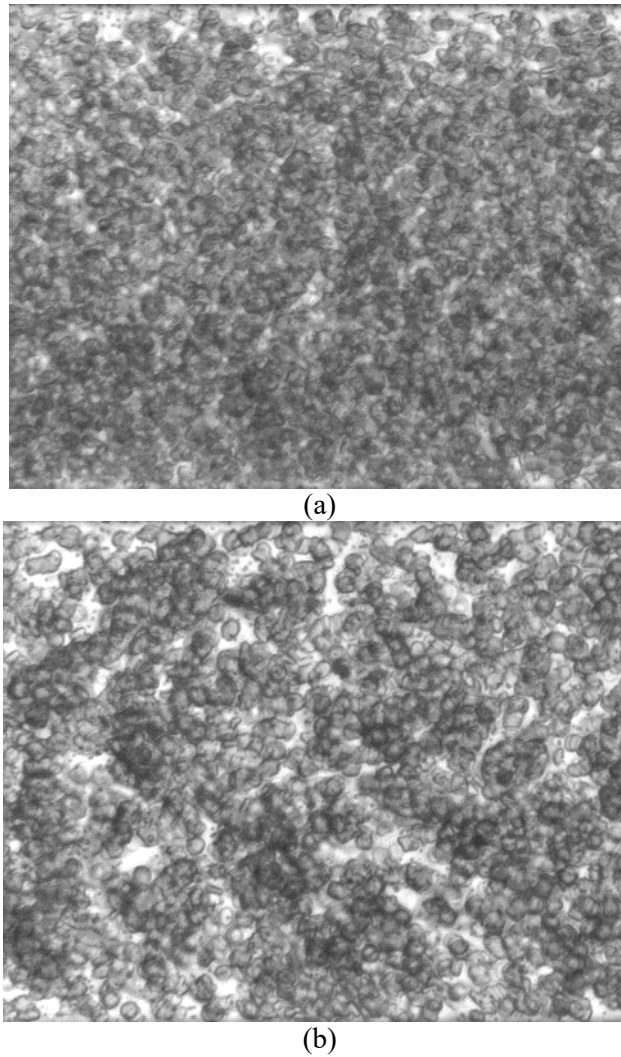enhanced absorption of light in the regions where there are dense aggregates.

(a)

(b)

Fig. 2. Images of aggregating blood, for (a) Re = 0.52 (no aggregation), and (b) Re = 0.02 (high aggregation).

Therefore, as shown in Figure 3, all three parameters increase for the more aggregating cases (i.e. as $Re \approx 0$). No aggregation is detected above $Re \approx 0.1$. The moderately and highly aggregated states have distinctly elevated levels of $\bar{I}'$, σ_I and n_s. The number of saturated pixels in the image (that is the pixels that have reached they maximum value in the measuring scale, i.e. white areas), as plotted in Fig.3(c), most sharply increases with aggregation and is a sensitive measure for highly aggregated states, although the calculated uncertainty was approximately 10 to 15 times greater than that for the other parameters. Note that the aggregation index used with previous aggregating blood velocity measurements in a plate-plate system [37,21] rely on the cells and aggregates flowing in an approximately two-dimensional manner, i.e. with little variation over the depth of the channel. This was not observed to be the case for the current study, where d = 50μm.
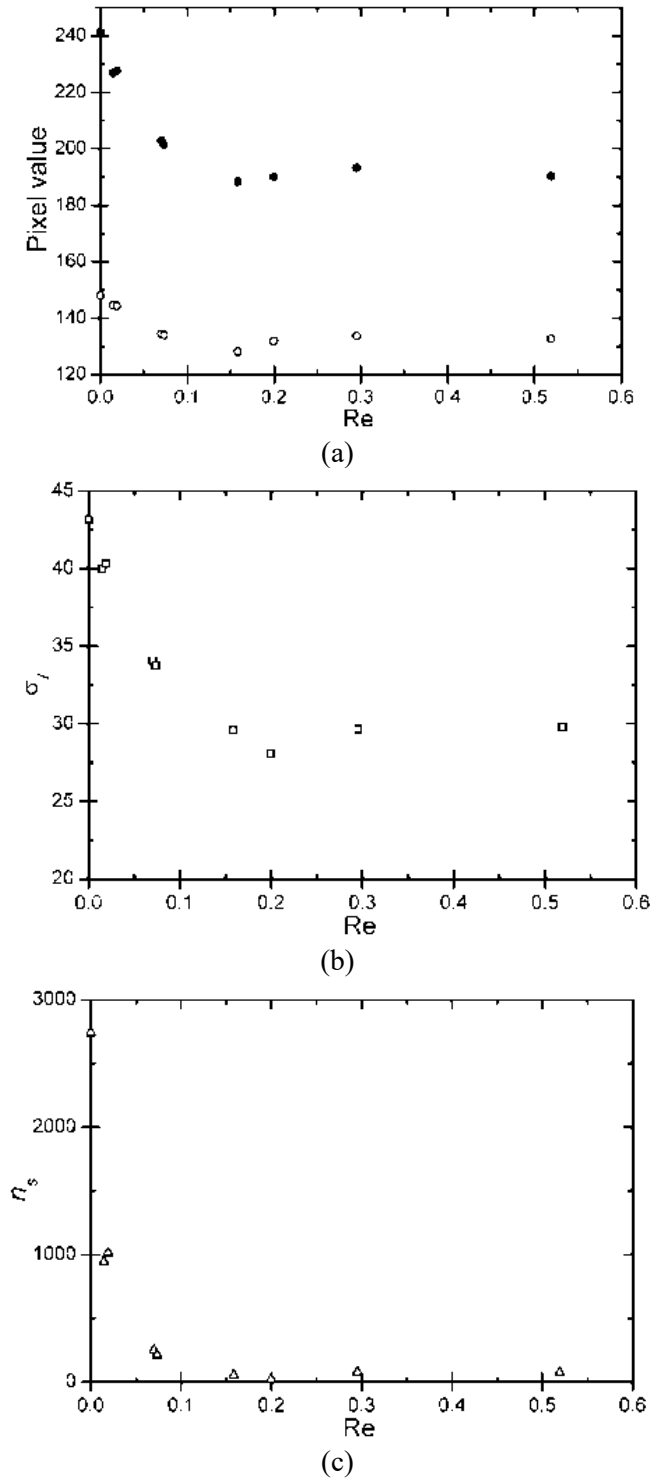
(a)

(b)

(c)

Fig. 3. Various image properties highlighting aggregation as a function of *Re* : (a) average pixel value for all pixels (open circles), and the brightest 10% of pixels (closed circles); (b) standard deviation of pixel intensity; and (c) average number of saturated pixels in each image.

Velocity vector fields derived from the brightfield images are presented in Fig.4. The three cases once again provide excellent examples of different degrees of aggregation and produced results which were replicated at similar *Re*. Velocities are normalised by maximum values of the average profile for each case to facilitate easy comparison between the three cases. The measured $\bar{U}$ values were 0.25, 1.0 and 6.8 mm/s for cases (a), (b), and (c), respectively. For *Re*=0.52 the velocity vector field is similar in appearance to the time-averaged vector field acquired using FMPIV (Fig. 1). However, local deviations

from this pattern appear for the cases with a higher degree of erythrocyte aggregation, particularly at *Re* = 0.02. These fluctuations occur in both space and time, and have been reported previously for flows within the plate-plate geometry with intense cell aggregation [21].
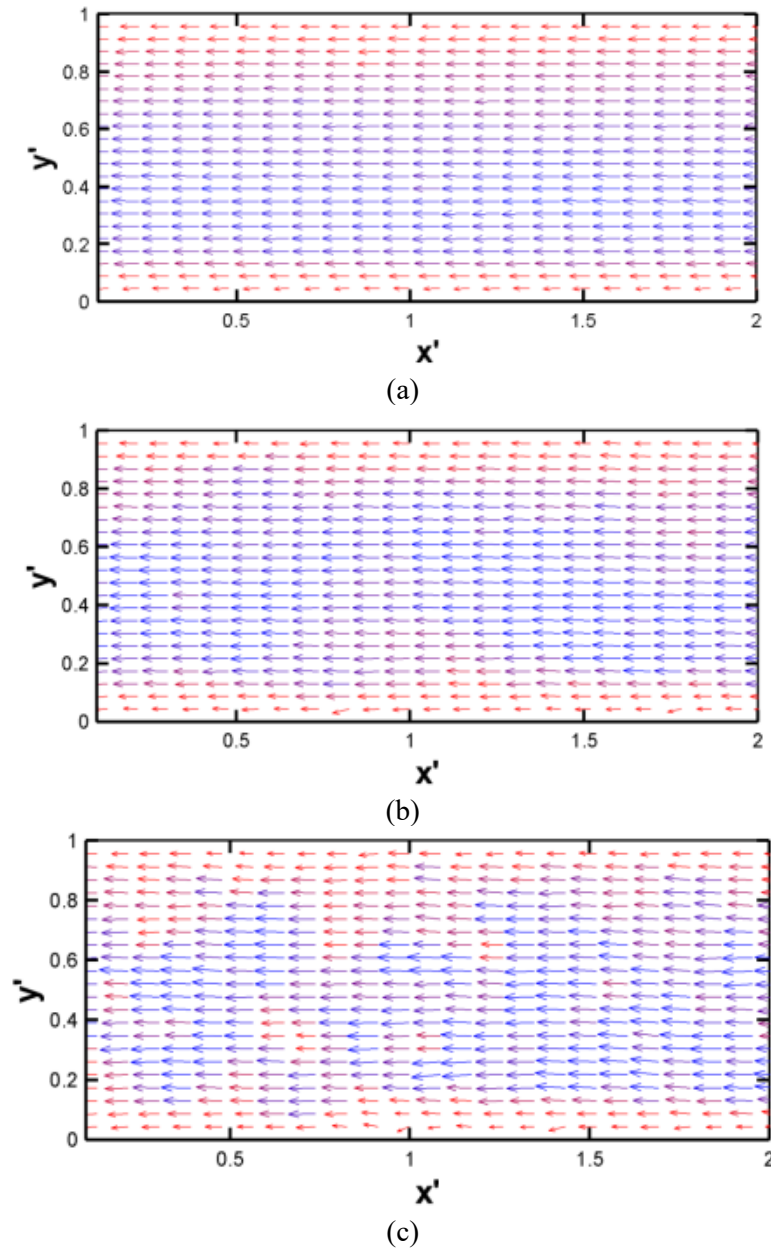

(a)

(b)

(c)

Fig. 4. Time-resolved velocity vector fields processed with 32×32 pixel windows, for (a)*Re* = 0.52 (no aggregation); (b) *Re* = 0.07 (moderate aggregation); and (c) *Re* = 0.02 (high aggregation). Colouring represents velocity magnitude. For clarity, every second vector in the *x* direction has been omitted.

Once aggregates exceed a certain size their transport through the narrow channels is more regularly impeded by interactions with the walls and other aggregates, leading to local, temporary decreases in velocity. For $|P_0|$. 0.3 kPaG we observed that the aggregates became stationary due to this effect. The altered velocity gradients result in even stronger local variations in shear, which itself could provide a feedback loop scenario whereby the aggregates themselves affected by the shear.
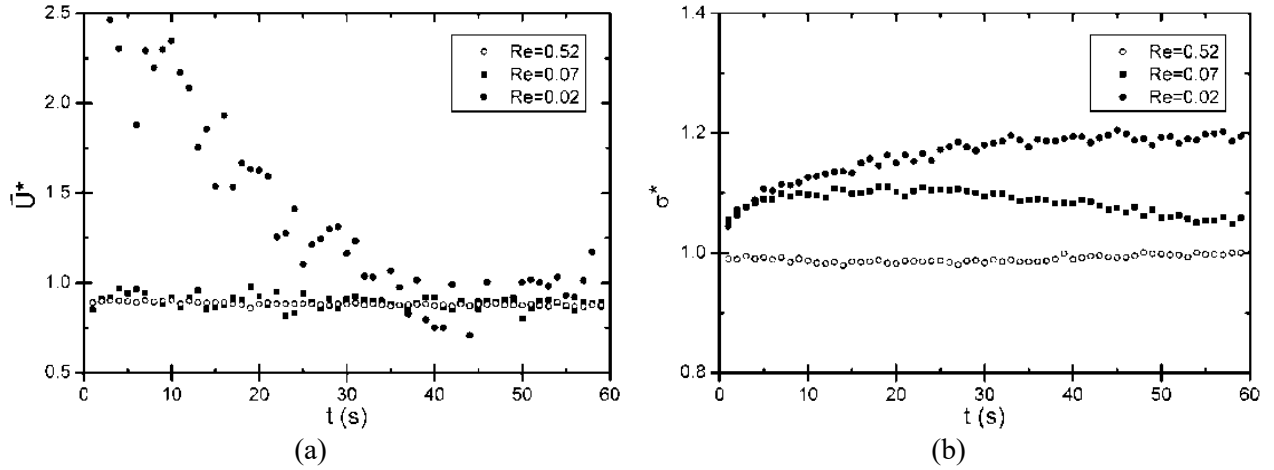
Fig. 5. (a) Time series of spatially averaged velocities for three different flow/aggregation cases, with values normalised by maximum velocity in the profile of the respective case. (b) Time series of standard deviation of pixel intensity for three different flow cases. Forcomparison purposes, all values shown are normalised by the final value of the $Re = 0.52$ case.

Sets of brightfield images were recorded every second for a full minute after P_0 was adjusted. Figures 5 (a) and 5(b) represent time series of mean velocity magnitude, and σ_I , respectively. Once again, the velocity values are normalised for ease of comparison. While the exact shape of the curves is specific for this particular blood sample and geometry, the plot provides an interesting view of time-dependent erythrocyte aggregation in flow. Both the non-aggregating ($Re=0.52$), and slightly aggregating ($Re = 0.07$) cases reach a flow rate close to the final value within a few seconds of being decelerated via a change of inlet pressure. The highly aggregating case ($Re = 0.02$), on the other hand, requires approximately 40 s to reach a steady flow rate. For this case the extent of aggregation, as denoted by pixel variance, also takes approximately 40 s to reach an approximate maximum level, and roughly follows the inverse of the trend of $\bar{U}^*$. For $Re = 0.07$ the behaviour combines aspects of both the highly aggregated and unaggregated cases. Here, σ_I increases to a maximum over the first 7 s, before decreasing very gradually, while $\bar{U}^*$ reaches a steady value within the first 2 or 3 s. This behaviour was observed for a repeated case at $Re = 0.07$. The scatter in the $\bar{U}^*$ values increases with aggregation, as is expected with greater variance in the velocity measurements. This difference is explained by a progressive increase in the tendency for cells to aggregate as shear rates decreases. For both aggregating cases, σ_I increases gradually to the maximum value, as aggregates require this period of time to reach full size.

3.3 Discussion and further technique evaluation

The results presented above highlight the capabilities of using BMPIV to probe the relationship between erythrocyte aggregation and flow profiles with high spatial and temporal resolution. In particular, the tendency for velocity fields of aggregating erythrocyte flow to deviate from the mean velocity profile is worth further consideration. This could be investigated by processing the images with smaller interrogation window sizes to increase measurement resolution. Figure 6 includes velocity profiles for the non-aggregating and highly aggregating cases obtained using a window size of 16×16 pixels, and a vector spacing of 8 pixels. While the individual measurement uncertainty is increased slightly, it is implied from the non-aggregating case (Fig 6(a)) that sufficient accuracy is achieved at this window size.
The local variations in the flow field of the aggregating case are highlighted more effectively using this measurement resolution. Features such as gap widening and interacting rouleaux are indicated, along with the size of a 32×32 pixel window (solid square) and a 16×16 pixel window (dashed square).
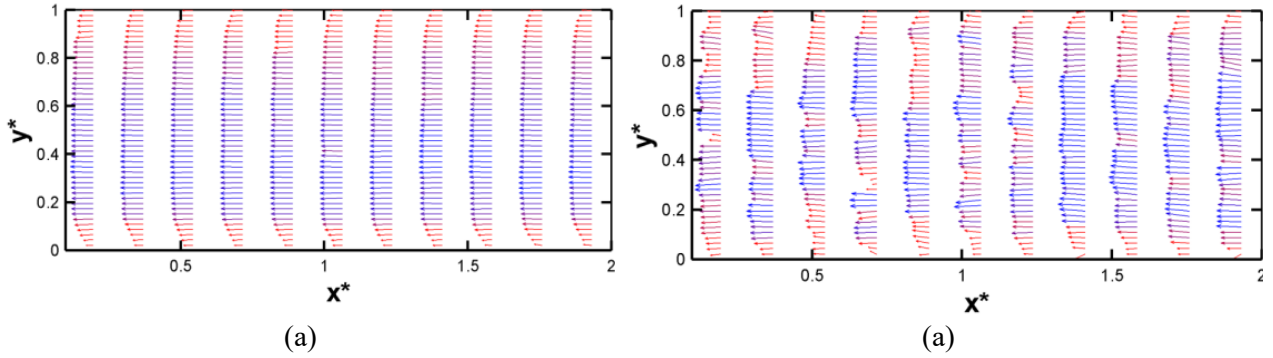
(a)　　　　　　　　　　　　　　　　　　(a)

Fig. 6. Time-resolved velocity vector fields processed with 16×16 pixel windows, for (a) *Re* = 0.52 (no aggregation); and (b) *Re* = 0.02 (high aggregation). Colouring represents velocity magnitude.

As a result of the strong correlation between aggregation and the degree of regional velocity variance, the PIV measurements themselves provide a quantitative indication of aggregation. The fluctuating component of the velocities ($\mathbf{u}'(x, y, t)$) was determined by subtracting the time and spatially averaged flow profile ($\mathbf{u}(y)$) from each of the velocity fields ($\mathbf{u}(x, y, t)$) in the last 10 s of acquisition, i.e. when the flow rate was steady. The standard deviation of the magnitude of these values, σ_v, is presented in Fig. 7 as a function of *Re*. The trends are similar to the brightness and contrast parameters shown in Fig. 2, with clear distinctions between the highly aggregated, moderately aggregated, and dispersed cell cases. Furthermore, a subtle decrease occurs in the region 0.15 . *Re* < 0.52, probably indicating small changes in aggregation over this range. Another possibility is a slight decrease in random measurement error, which would also be reflected in the value of $\mathbf{u}'(x, y, t)$, however this is unlikely as the cell images in this range are of similar appearance.
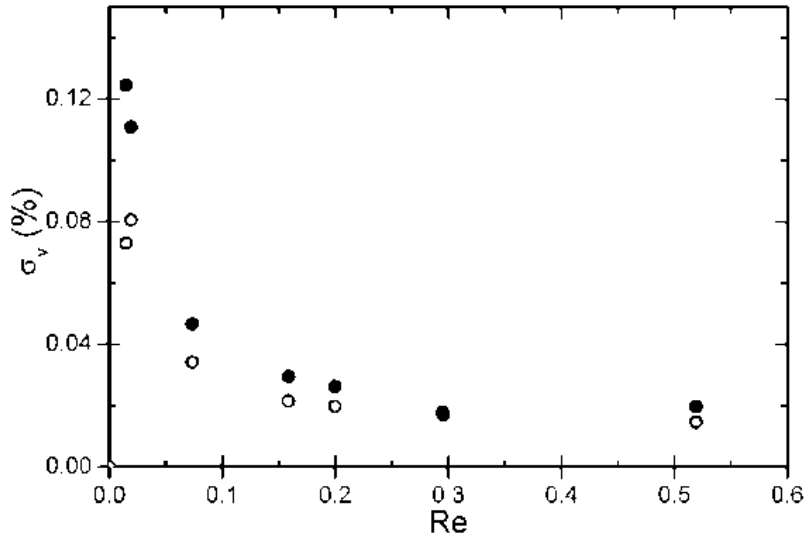

Fig. 7. Standard deviation of normalised velocity magnitude as a function of *Re*, processed using 32×32 pixel windows (open circles) and 16×16 pixel windows (closed circles)

Use of brightfield microscopy for micro-PIV measurements of blood flows is not new, however the present study strongly demonstrates the usefulness and robustness of this approach for quantifying the flow of erythrocytes, particularly where aggregation is present. An obvious benefit of BMPIV is that it does not require a high-sensitivity camera, a laser, or an epi-fluorescent system optics, all of which are necessary for FMPIV. The relative simplicity and safety of the experimental configuration, and the widespread availability of PIV processing software, means that this approach could potentially be developed as a practical tool for analysis of the aggregation and flow resistance properties of patient blood samples in lab-on-a-chip biomedical devices.

4 Conclusions

The manner in which erythrocyte aggregation affects flow behaviour, thereby influencing the broader rheological properties of blood, is an area of haemodynamics which has significant knowledge gaps, despite its relevance to pathological conditions. In the current study, microscope imaging techniques have been used to simultaneously describe the state of cell aggregation within a blood sample flowing through a microchannel, as well as the corresponding velocity fields. For higher flowrate cases, in which cells are dispersed, the time-resolved velocity profiles acquired using BMPIV are consistent with those those measured using FMPIV. As the flowrate approaches zero, however, the cells begin to aggregate, which affects the velocity fields. Local spatial and temporal deviations from the expected velocity profiles increase with aggregation, which is primarily due to the interaction of erythrocyte aggregates with each other and the channel walls. The image properties (e.g. brightness, contrast, saturation level) and the velocity variance both provide quantitative indications of the presence of aggregation at different levels, which could be further developed for research and medical purposes. An important next step will be to apply this approach to study aggregating blood flow through microchannel geometries which more closely resemble the microvasculature.

References

[1] Almog, B. Gamzu, R. Almog, R. Lassing, J. Shapira, I. Berliner, S. Pauzner, D. Maslovitz, I. Levin, S., 2005. Enhanced erythrocyte aggregation in clinically diagnosed pelvic inflammatory disease. Sexually Transmitted Diseases 32 (8), 484–486.

[2] Berliner, S. Ben-Ami, R. Samocha-Bonet, D. Abu-Abeit, S. Schechner, V. Beigek, Y. Shapira, I. Yedgar, S. Barshtein, G., 2004. The degree of red blood cell aggregation on peripheral blood glass slides corresponds to inter-erythrocyte cohesive forces in laminar flow. Thrombosis Research 114, 37–44.

[3] Ben-Ami R., Barshtein G., Mardi T., et al. A synergistic effect of albumin and fibrinogen on immunoglobulin-induced red blood cell aggregation. *The American Journal of Physiology—Heart and Circulatory Physiology*. 2003;285(6):H2663–H2669.

[4] Meiselman, H., 2009. Red blood cell aggregation: 45 years being curious. Biorheology 46, 1–19.

[5] Rampling, M., 1989. Red cell aggregation and yield stress. Clinical Blood Rheology 1, 45–63.

[6] Rampling, M.W. Meiselman, H Neu, B. Baskurt, O. K. 2004. Influence of cell specific factors on red blood cell aggregation. Biorheology 41 (2), 91–112.

[7] Picart, C. Piau, J.-M. Galliard, H. Carpentier, P.,1998. Blood low shear rate rheometry: influence of fibrinogen level and hematocrit on slip and migrational effects, Biorheology 35 (4-5), 335–353.

[8] Bishop, J., Nance, P., Popel, A., Intaglietta,M., Johnson, P., 2001. Effect of erythrocyte aggregation on velocity profiles in venules. American Journal of Physiology : Heart and Circulatory Physiology 280, H222–H236.

[9] Cokelet, G., 1999. Viscometric, in vitro and in vivo blood viscosity relationships: how are they related? Biorheology 36, 343–358.

[10] Cokelet, G., Goldsmith, H., 1991. Decreased hydrodynamic resistance in the twophase flow of blood through small vertical tubes at low flow rates. Circulation Research 68, 1–17.

[11] Reinke, W., Gaehtgens, P., Johnson, P., 1987. Blood viscosity in small tubes: effect of shear rate, aggregation, and sedimentation. American Journal of Physiology :Heart and Circulatory Physiology 253, Iss.3, H540 –H547.

[12] Babu, N., Singh, M., 2004. Influence of hyperglycemia on aggregation, deformability and shape parameters of erythrocytes. Clinical Hemorheology and Microcirculation 31, 273–280.

[13] Barabino, G., Platt, M. O., Kaul, D., 2010. Sickle cell biomechanics. Annual Review of Biomedical Engineering 12, 345–367.

[14] Forconi, S., Gori, T., 2009. The evolution of the meaning of blood hyperviscosity in cardiovascular physiopathology: Should we reinterpret Poiseuille? Clinical Hemorheology and Microcirculation 42, 1–6.

[15] Froom, P., 2000. Blood viscosity and the risk of death from coronary heart disease. European Heart Journal 21, 513–514.

[16] Intaglietta, M., 2009. Increased blood viscosity: Disease,adaptation or treatment? Clinical Hemorheology and Microcirculation 42, 305–306.

[17] Smith,M., Chen, P., Li, C.-S., Ramanujam, S., Cheung, A., 2009. Whole blood viscosity and microvascular abnormalities in alzheimers disease. Clinical Hemorheology and Microcirculation 41, 229–239.

[18] Baskurt, O., Uyuklu, M., Ulker, P., Cengiz, M., Nemeth, N., Alexy, T., Shin, S., Hardeman,M., Meiselman, H., 2009b. Comparison of three instruments for measuring red blood cell aggregation. Clinical Hemorheology and Microcirculation 43, 283–298.

[19] Shin, S., Park, M., Ku, Y., Suh, J., 2006. Shear-dependent aggregation characteristics of red blood cells in a pressure-driven microfluidic channel. Clinical Hemorheology and Microcirculation 34, 353–361.

[20] Baskurt, O., Bonyard, M., Cokelet, G., P., C., Cooke, B., Forconi, S., Liao, F., Hardeman,M., Jung, F.,Meiselman, H., Nash, G., Nemeth, N., Neu, B., Sandhagen, B., Shin, S., Thurston, G., Wautier, J., 2009a. New guidelines for hemorheological laboratory techniques. Clinical Hemorheology and Microcirculation 42, 75–97.

[21] Dusting, J., Kaliviotis, E., Balabani, S., Yianneskis, M., 2009. Coupled human erythrocyte velocity field and aggregation measurements at physiological haematocrit levels. Journal of Biomechanics 42, 1438–1443.

[22] Santiago, J., Wereley, S., Meinhart, C., Beebe, D., Adrian, R., 1998. A particle image velocimetry system for microfluidics. Experiments in Fluids 25, 316–319.

[23] Vennemann, P., Lindken, R.,Westerweel, J., 2007. In vivo whole field blood velocity measurement technique. Experiments in Fluids 42, 495–511.

[24] Ji, H., Lee, S., 2008. In vitro hemorheological study on the effect of human blood flow in a microtube. Clinical Hemorheology and Microcirculation 40, 19–30.

[25] Lima, R.,Wada, S., Takeda,M., Tsubota, K., Yamaguchi, T., 2007. In vitro confocal micro-PIV measurements of blood flow in a square microchannel: The effect of the haematocrit on instantaneous velocity profiles. Journal of Biomechanics 40, 2752–2757.

[26] Nakano, A., Sugii, Y., Minamiyama, M., Niimi, H., 2003. Measurement of red cell velocity in microvessels using particle image velocimetry (PIV). Clinical Hemorheology and Microcirculation 29, 445–455.

[27] Poelma, C., Van der Heiden, K., Hierck, B., Poelmann, R., Westerweel, J., 2009. Measurements of the wall shear stress distribution in the outflow tract of an embryonic chicken heart. Journal of the Royal Society Interface 7 (42), 91–103.

[28] Savery, M., Damiano, E., 2008. The endothelial glycocalyx is hydrodynamically relevant in arterioles throughout the cardiac cycle. Biophysical Journal 95, 1439–1447.

[29] Soutani, M., Suzuki, Y., Tateishi, N., Maeda, N., 1995. Quantitative evaluation of flow dynamics of erythrocytes in microvessels: influence of erythrocyte aggregation. American Journal of Physiology: Heart and Circulatory Physiology 268, H1959–H1965.

[30] Sugii, Y., Okuda, R., Okamato, K., Madarame, H., 2005. Velocity measurement of both red blood cells and plasma of in vitro blood flow using high-speed micro piv technique. Measurement Science and Technology 16, 1126–1130.

[31] Vennemann, P., Kiger, K., Lindken, R., Groenendijk, B., Stekelenburg-de Vos, S., ten Hagen, T., Ursem, N., Poelmann, R.,Westerweel, J., Hierck, B., 2006. In vivo micro particle image velocimetry measurements of blood-plasma in the embryonic avian heart. Journal of Biomechanics 39, 1191–1200.

[32] Lipowsky, H., 2005. Microvascular rheology and hemodynamics. Microcirculation 12, 5–15.

[33] Lipowsky, H., Kovalcheck, S., Zweifach, B., 1978. The distribution of blood rheological parameters in the microvasculature of cat mesentery. Circulation Research 43, 738–749.

[34] Lipowsky, H., Usami, S., Chien, S., 1980. In vivo measurements of apparent viscosity and microvessel hematocrit in the mesentery of the cat. Microvascular Research 19, 297–319.

[35] Fung, Y., 1997. Biomechanics: Circulation. 2*nd* edition. Springer.

[36] Barbee, J., Cokelet, G., 1971. The fahraeus effect.Microvascular Research 3, 6–16.

[37] Kaliviotis, E., Yianneskis, M., 2008. On the effect of microstructural changes of blood on energy dissipation in couette flow. Clinical Hemorheology and Microcirculation 39, 235–242.